Article

Understanding the Role of Molecular Diffusion and Catalytic Selectivity in Liquid-Phase Beckmann Rearrangement

Matthew E. Potter, Alexander J. O'Malley, Stephanie Chapman, Julija Kezina, Stephanie H. Newland, Ian P Silverwood, Sanghamitra Mukhopadhyay, Marina Carravetta, Thomas M Mezza, Stewart F. Parker, C. Richard A. Catlow, and Robert Raja

ACS Catal., **Just Accepted Manuscript** • DOI: 10.1021/acscatal.6b03641 • Publication Date (Web): 13 Mar 2017

Understanding the Role of Molecular Diffusion and Catalytic Selectivity in Liquid-Phase Beckmann Rearrangement

*Matthew E. Potter,[a] Alexander J. O'Malley,[b,c] Stephanie Chapman,[a] Julija Kezina,[a,d] Stephanie H. Newland,[a] Ian P. Silverwood,[c,e] Sanghamitra Mukhopadhyay,[e] Marina Carravetta,[a] Thomas M. Mezza,[f] Stewart F. Parker,[c,e] C. Richard A. Catlow[b,c,g] and Robert Raja[a,c]**

a. School of Chemistry, University of Southampton, University Road, Southampton, SO17 1BJ, UK.

b. Department of Chemistry, University College London, 20 Gordon Street, London WC1H 0AJ, UK.

c. UK Catalysis Hub, Research Complex at Harwell, Science and Technology Facilities Council Rutherford Appleton Laboratory, Harwell Science and Innovation Campus, Oxon OX11 0QX, UK.

d. Analytical Sciences and Development, GSK, Medicines Research Centre, Gunnels Wood Road, Stevenage, Hertford-shire, SG1 2NY, UK.

e. ISIS Pulsed Neutron and Muon Facility, Science and Technology Facilities Council Rutherford Appleton Laboratory, Harwell Science and Innovation Campus, Oxon OX11 0QX, UK.

f. UOP LLC, A Honeywell Company, 25 East Algonquin Road, Des Plaines, IL 60017, USA.

g. Cardiff Catalysis Institute, School of Chemistry, Cardiff University, UK.

ABSTRACT

Understanding the role of diffusion in catalysis is essential in the design of highly active, selective and stable industrial heterogeneous catalysts. By using a combination of advanced *in situ* spectroscopic characterisation tools, particularly quasi-elastic and inelastic neutron scattering, we outline the crucial differences in diffusion modes and molecular interactions of active sites within solid-acid catalysts. This, coupled with 2D solid-state NMR and probe-based FTIR spectroscopy, reveals the nature of the active site in our SAPO-37 catalyst and affords detailed information on the evolution of solid-acid catalysts that can operate at temperatures as low as 130 °C, for the Beckmann rearrangement of cyclohexanone oxime to ε-caprolactam (precursor for Nylon-6). The versatility of this approach leads to structure-property correlations that contrast the dynamics of the diffusion process in the different materials studied. Our results illustrate the power of these techniques in unravelling the interplay between active site and molecular diffusion in single-site heterogeneous catalysts, which can play a vital role in designing low-temperature, sustainable catalytic processes.

KEYWORDS

Neutron scattering, catalytic diffusion, Beckmann rearrangement, heterogeneous catalysts, nylon-6, operando spectroscopy.

INTRODUCTION

The ability to mimic the catalytic function of natural enzymes and tailor a robust structural environment, akin to the protein tertiary structure, to overcome complex mass-transport and diffusion limitations, has long been a goal of synthetic chemists.[1,2] Microporous zeotype architectures have proved particularly effective in facilitating diffusion in catalysts, where molecular transport can be controlled through a range of interconnecting channels and cages.[3,4] It is further possible to devise synthetic procedures to target the formation of active sites that deliver a specific catalytic function (analogous to enzymes).[5-10] This has enabled Brønsted and Lewis[11-13] sites to be engineered within these frameworks, making them efficient and versatile solid acid catalysts within the petrochemical industry.[5,14,15] Despite the range of zeotype frameworks known, only a few are industrially exploited (MFI (ZSM-5), FAU (Zeolite-Y), CHA (SAPO-34), etc.). Unlike enzymes that operate at ambient to low-temperatures, these inorganic analogues require higher temperatures, often in excess of 350 °C, to overcome mass-transport limitations and yield higher activity (potentially compromising selectivity, atom efficiency and catalyst stability).[16,17] The scope therefore for designing low-temperature, solid-acid catalysts for the Nylon-6 industry (predicted to be valued at 14 billion USD in 2019), that can catalyse the Beckmann rearrangement of cyclohexanone oxime to ε-caprolactam (global production of 4.9 million tonnes in 2014) with high activities and selectivities is highly desirable.[18]

Despite the importance of diffusion processes in controlling reaction pathways and mechanisms, the role of diffusion and transport in nanoporous solids is typically studied to a lesser extent than the active site.[19] The dynamic behaviour of cyclohexanone oxime within the channels of zeotype architectures in the Beckmann rearrangement is not clearly understood. Studies on ZSM-5 suggest the restrictive framework forces the reaction to occur on the catalyst's surface and in the periphery of the pore mouth,[20-25] while the constricting micropores promote the formation of ring-opening by-products.[22-25] Conversely, others have employed *in situ* infrared techniques to emphasise that the internal acid sites predominantly yield the lactam.[24,25] Therefore, unsurprisingly, it is challenging to understand a reaction process while separating the influences of molecular diffusion and the nature of the active site. To facilitate a more holistic understanding, we present a combined catalytic and multi-technique characterisation study (employing *in situ* techniques) investigating the catalysed, liquid-phase Beckmann rearrangement of cyclohexanone oxime using a tailored SAPO-37 (aluminophosphate analogue of the zeotype FAU) architecture, with controlled acid site concentration.[15]

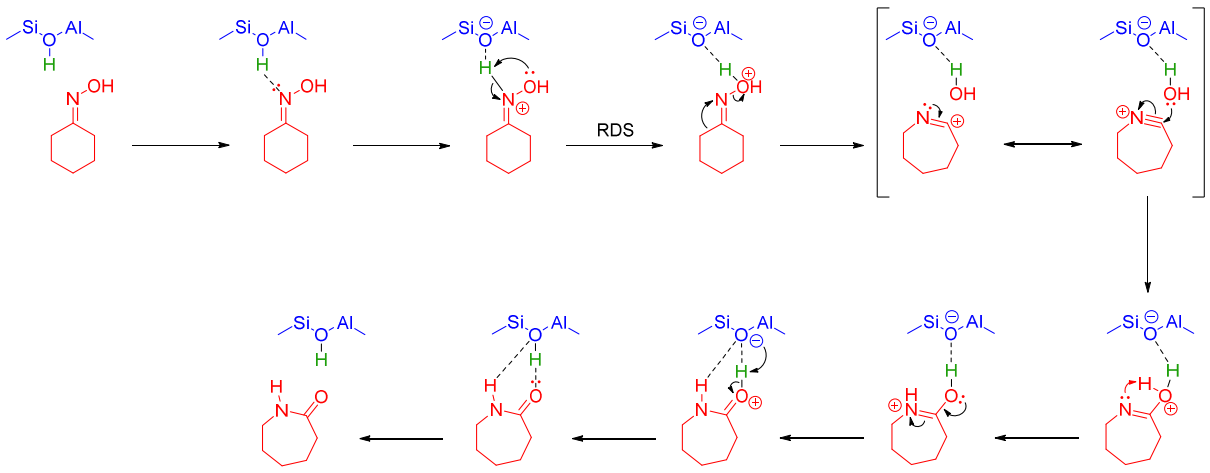

Scheme 1. Typical mechanistic pathway for the acid-catalysed Beckmann rearrangement of cyclohexanone oxime.

To ensure meaningful comparisons, parallel studies were also performed on Zeolite-Y (FAU), to facilitate detailed structure-property correlations and explore the interplay between active-site structure and molecular diffusion within the same FAU architecture. For the sake of completeness, we also probed the efficacy of the (conventionally used) ZSM-5 catalyst[20,26] in the liquid-phase Beckmann rearrangement of cyclohexanone oxime to contrast the influence of pore aperture with our SAPO-37 analogue. In particular, we present the use of quasi-elastic neutron scattering (QENS), which has been shown to effectively characterise and quantify diffusion of confined hydrocarbons,[27,28] and was recently used in tandem with vibrational spectroscopy to gain insight into key steps of the zeolite-catalysed methanol-to-hydrocarbons process in commercial catalysts.[29] Here we directly study the dynamics of the reactant, cyclohexanone oxime to determine the nature of the diffusion in the liquid-phase Beckmann rearrangement which, coupled with inelastic neutron scattering (INS), solid-state 2D NMR, and probe-based FTIR spectroscopy, offers valuable insights into the specific role played by solid-acid sites in the mechanistic and reaction pathways (Scheme 1).[21] The QENS study further supports our design rationale of combining a specific active site with a specific framework topology to create an effective catalyst, which affords near quantitative yields of ε-caprolactam at temperatures as low as 130 °C.

EXPERIMENTAL METHODS

QENS Methodology

All QENS measurements were performed using the high resolution time-of-flight (TOF) instrument OSIRIS at the ISIS neutron source, Chilton, Oxfordshire. The analyzer crystals used were cooled pyrolytic graphite (PG002) with the energy transfers measured in a window of

±0.61 meV. The energy resolution of this instrument with this configuration in near back-scattering geometry is 24.5 μeV. The samples (4.5 grams each in total) were transferred inside a glove box, after drying, to cylindrical aluminium containers of annular geometry. The cells were placed in a CCR cryostat so that a resolution measurement could be taken at 30 K. The measurements were then taken at 373 K. The signal taken from an empty zeolite was taken pre-loading and then subtracted from the signal of the loaded zeolite so that only the signal from the oxime was measured.

Inelastic Neutron Scattering Spectroscopy

The SAPO-37 was dried under a flow of He gas at 550 °C for 2 hours. A 1:10 solid-state mixture of cyclohexanone oxime and SAPO-37 was prepared in a glove box, under argon atmosphere. The mixture was transferred to an aluminium-foil sachet, which was sealed in an aluminium can. The experiments were carried out using the high resolution, INS spectrometer MAPS at the ISIS Pulsed Neutron and Muon Source (Oxfordshire, UK). The cans were placed in a top-loading, closed cycle refrigerator cryostat, all spectra were collected at < 30 K in order to minimize the Debye-Waller factor. Measurements were taken at neutron incident energies of 650 meV ('A' chopper speed 600 Hz), 250 meV ('A' chopper speed 400 Hz) and 100 meV ('A' chopper speed 200 Hz).

RESULTS AND DISCUSSION

The framework integrity of the SAPO-37, Zeolite-Y and ZSM-5 was determined *via* a range of techniques. Powder XRD patterns of the three samples (Figure S1) show that all materials are highly crystalline and phase-pure, suggesting an ordered structure with minimal defects. The crystallinities were compared with respect to a potassium iodide standard and showed that Zeolite-Y and SAPO-37 have very similar levels of crystallinity (Figure S1). Particle size is also known to influence diffusion in porous materials and scanning electron microscopy (SEM, Figure S2) revealed the presence of uniform particles (1 μm in size), in all three catalysts. The exterior of the particles appeared smooth and regular in all cases, suggesting similar levels of surface defects (Figure S2). Finally, N_2 physisorption isotherms showed good agreement between the Zeolite-Y and SAPO-37 frameworks for surface area and micropore volume, (Table S1), which was in good agreement with the literature values.[29,30] It is important to note that similar levels of dopant species (Al for zeolites, Si for SAPO-37) were deliberately introduced in all three catalysts (Table S1), to ensure meaningful comparisons can be established for contrasting the influence of the dopant substitution on active-site formation.

Quasi-elastic neutron scattering (QENS) was used to monitor the molecular motion of cyclohexanone oxime within the inorganic zeotypes, at temperatures (373 K) akin to the liquid-phase catalytic experiments (experimental limitations restrict the use of higher temperatures). A more rigorous discussion of QENS theory can be found in the ESI, and is summarised below. Hydrogen has the largest incoherent scattering cross-section of any element,[31] so is the primary contributor to the experimentally-measured incoherent scattering function; $S(\mathbf{Q},\omega)$, allowing the oxime to be observed in the presence of the prominent inorganic matrix. Molecular motions perturb elastic neutron-matter interactions, causing quasi-elastic deviations that result in a quantifiable broadening of the elastic line. For isotropic diffusion, the broadening of $S(\mathbf{Q},\omega)$, is

described as a Lorentzian function, linking the half-width half-maximum (HWHM) of the quasi-elastic component, $\Delta\omega(Q)$, to the self-diffusion coefficient D_s, and momentum transfer vector Q ($Å^{-1}$) between the incident and scattered neutron, where ω is neutron energy transfer (meV).[31-33]

$$\Delta\omega(Q) = D_s Q^2 \qquad \text{(Eq. 1)}$$

Different models are needed for non-Fickian behaviour, such as the Chudley-Elliot model,[33] where a molecule is temporarily immobilised before jumping to the next site. These models include derivable parameters such as residence time and jump distance.[33] The QENS spectra of cyclohexanone oxime in ZSM-5 (Figure S3) closely match the Gaussian instrument resolution function at lower Q values, with no observable quasi-elastic component, indicating no long range translational diffusion is observable over the time and length scales accessible to the spectrometer at these temperatures.[34] A minimal Lorentzian component is observed at the higher Q values,[35,36] As we cannot detect any broadening at low momentum transfers, it is difficult to say whether these broadenings may be associated with rotational motion, or indeed conform to the higher Q behavior of a jump diffusion model. Regardless, this component is too small for reliable analysis, and a spectrometer of higher resolution, able to detect motion over longer timescales, would be necessary to characterize or quantify any mobility in this system. However, the minimal quasi-elastic component indicates that any translational diffusion occurring would be much slower than can be detected here.[37] It is plausible that the channel dimensions (5.5 Å) are too small to allow significant diffusion of the cyclohexanone oxime (sorbate) at these temperatures, thus internal active sites cannot be accessed for this catalyst under these conditions. (It has been shown that such sites may be accessible under vapour-phase conditions (> 300 ^{o}C),[24,25] which is outside the scope of the current study).

Spectra obtained for the sorbate in both Zeolite-Y and SAPO-37 for four Q values are depicted in Figure S4 and Figure 1, respectively. The error in the neutron data points in Figures 1, S3 and S4 are assigned based on Poisson statistics. All spectra were fit with a resolution function, a single Lorentzian function describing the quasi-elastic component and a flat background, suggesting one dominant motion is present on the instrument timescale. The Lorentzian component obtained for Zeolite-Y (Figure S4) showed continuous broadening, whereas SAPO-37 only showed broadening up to a Q value of ~ 1.2 Å^{-1} (Figure 1). The error in the Lorentzian HWHM fits are assigned using a Monte Carlo method, where data sets are generated virtually within the neutron data point error bars and then fitted.

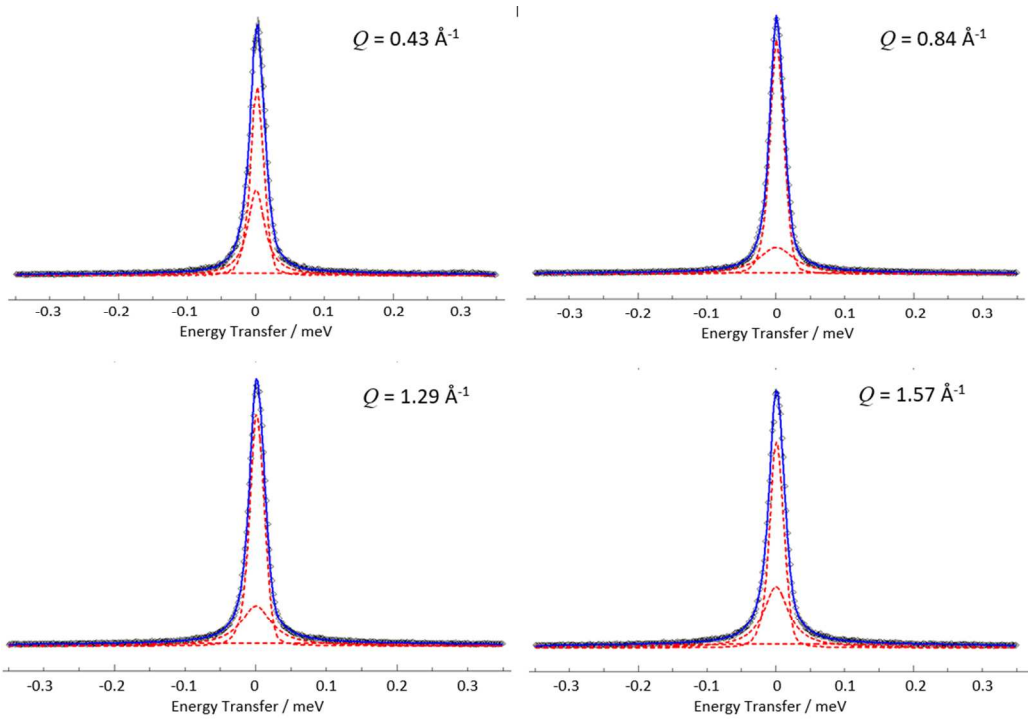

Figure 1. QENS spectra obtained for cyclohexanone oxime diffusing in SAPO-37 at four different Q values at 373 K, showing the total fit (blue), the constituent resolution; Lorentzian and flat background functions (red).

The HWHM broadening in Zeolite-Y shows a DQ^2 dependence, consistent with Fickian diffusion (Figure 2a), indicating the oxime moves freely through the microporous framework (diffusion coefficient of $2x10^{-10}$ ($\pm$ 0.18 x 10^{-10}) m^2 s^{-1}).[38] The SAPO-37 Q dependence is not linear (Figure 2b), but follows the Chudley-Elliot model for jump diffusion (a jump mechanism was previously observed for benzene in Na-Y)[33] with a jump distance of 4.5 Å and a residence time of 50 ps (Figure 2). This leads to an extrapolated diffusion coefficient of 6.5 x 10^{-10} ($\pm$ 2.7 x 10^{-10}). We note that while the higher D_s approximated from the jump model is an interesting observation, the different mechanisms from which these values are calculated, and the significantly higher errors associated with the jump model mean that a direct comparison of the two values must be treated with caution. The observed jump distance (4.5 Å) matches the length of a window region within the faujasite structure, showing the sorbate residing in one supercage before jumping into a neighbouring cage; this result suggests that the oxime is able to diffuse through the internal pores (at these low temperatures), accessing the internal acid sites. The tendency of the oxime to reside in certain areas of the SAPO-37 framework derives from the interactions with the internal acid sites. These interactions would potentially yield a greater production of lactam than in Zeolite-Y, which allows Fickian diffusion of the reactant, (suggesting minimal interactions between the oxime and acid sites). The constrained nature of the motion may also be attributed to pore-occlusion. Acid sites which are located at the pore mouths may interact with the oxime molecule, preventing it from accessing the pores. These findings were also independently verified by carrying out separate catalytic tests that mimic the experimental conditions and setup as outlined in Figure 2 (90% catalyst, 10% oxime, 373 K, 8 hours, solvent-free, under nitrogen environment) for all three catalysts. We did not observe any appreciable (< 5 mol%) conversion at 373 K in all three cases, which vindicates our conclusion

that any QENS signal is predominantly due to the cyclohexanone oxime. The reactant has therefore a differing diffusion mechanism at this temperature via jump-diffusion but does not react.

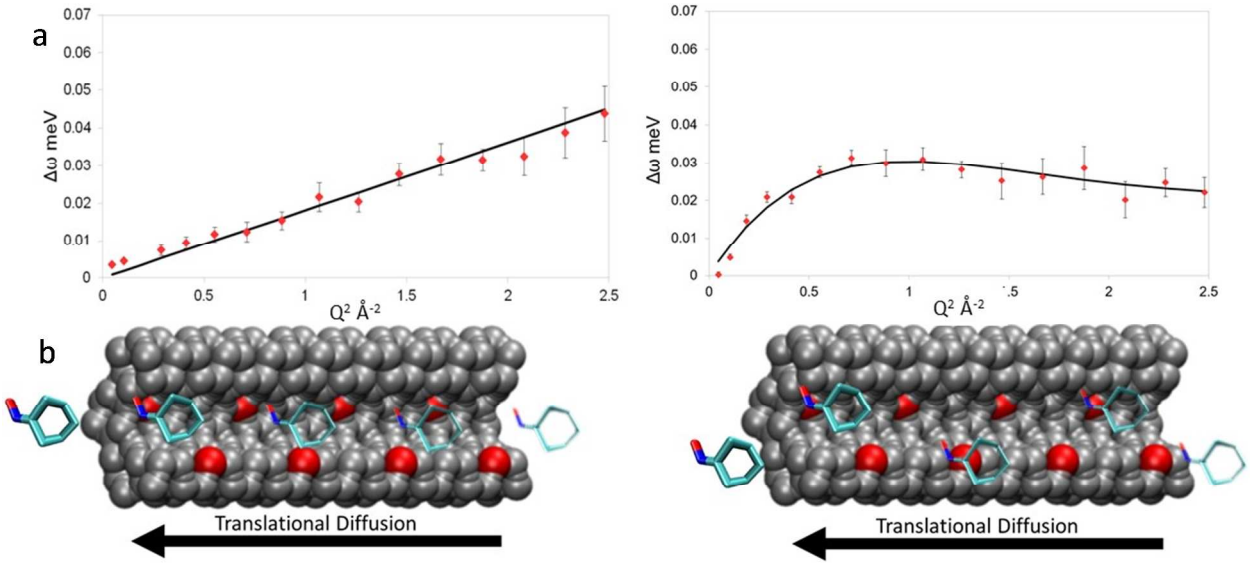

Figure 2 (a) The *Q*-dependence of the HWHM of the Lorentzian for Zeolite-Y (left) and SAPO-37 (right) at 373 K. (b) Contrasting diffusion modes of cyclohexanone oxime flowing through a pore with active sites (red): the oxime moves straight through the pore when there is a smooth Fickian diffusion (left with Zeolite-Y) and the oxime shifts between active sites with a specific residence time during jump diffusion (right with SAPO-37).

To understand better the change in diffusional behaviour, an inelastic neutron spectroscopy study (INS) was performed. INS spectra are similarly dominated by modes involving hydrogen motion; therefore the spectra largely reflect the hydrogenous component present. Figure 3a shows the O–H stretching region of SAPO-37 (4000 – 2000 cm^{-1}), before and after introduction of the oxime. Interestingly, the O–H stretch of the framework hydroxyls (3650 cm^{-1}) has been severely reduced. This demonstrates a significant interaction between the SAPO-37 and the

oxime, in keeping with the observed jump diffusion in the QENS. Focussing on a lower energy range (1600 – 800 cm^{-1}, Figure 3b) provides more detailed insights into the oxime-SAPO-37 interactions. Contrasting pure cyclohexanone oxime (black line, Figure 3b) with cyclohexanone oxime combined with SAPO-37 (pink line, Figure 3b), several peaks recede. Most notably this occurs in the 1600 – 1500 cm^{-1} region and the 1050 – 950 cm^{-1} region. These peaks are assigned as O-H vibrations from DFT based CASTEP calculations.[39,40] The other peaks (attributed to C-H vibrations through the same calculations) remain comparatively constant. The SAPO-37 O-H bend at 1060 cm^{-1} has receded, most likely upshifted due to hydrogen-bonding interactions with the oxime, and may be enveloped by the intense ring deformation modes surrounding it. This observation suggests that the oxime is indeed interacting with the acid sites of the SAPO-37 *via* the OH group of the oxime (as seen by the disappearance of both signals in the INS, Figures 3a and 3b), in keeping with the suggested mechanism (Scheme 1).

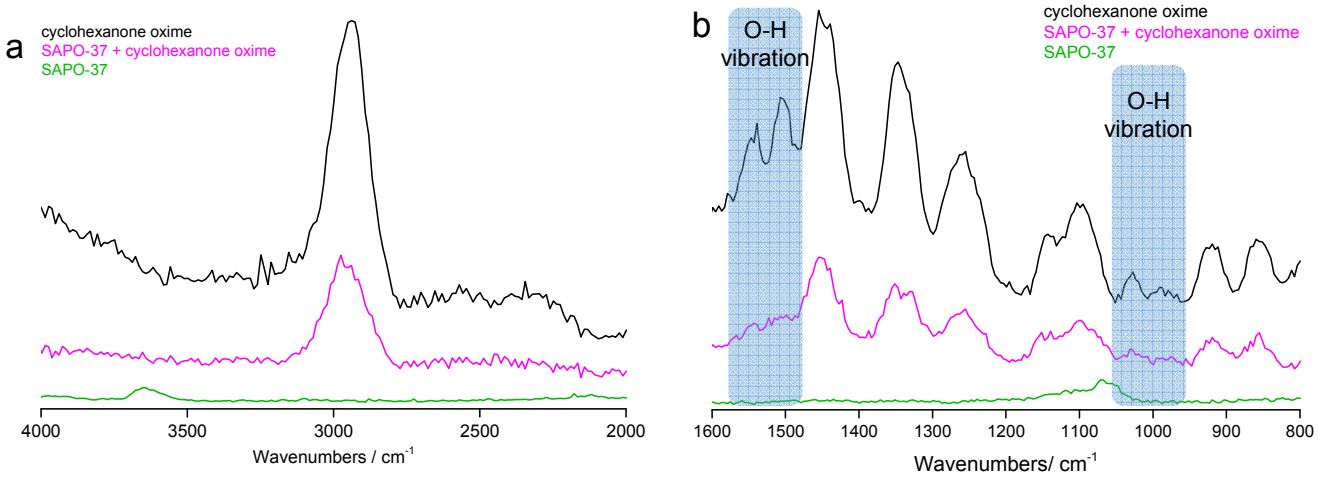

Figure 3 INS vibrational spectra showing the influence of oxime binding to SAPO-37. (a) E_i = 650 meV, the Brønsted acid peak in SAPO-37 (3650 cm^{-1}) is removed on addition of the oxime showing the interactions between the two. (b) E_i = 250 meV, shows the reduction in the O-H vibration bands relative to the ring deformation modes.

The combined INS and QENS data reveal fascinating contrasts between the three catalysts. In ZSM-5, the reactant is unable to access the internal pores under these timescales, while in Zeolite-Y, the molecules diffuse freely through the pore, and therefore do not interact with the solid-acid sites at 373 K. In SAPO-37, the enhanced interaction, as seen through INS, (facilitated by the nature, type and strength of acid centres within the internal pores, as discussed later) with these sites results in jump diffusion at lower temperatures, which is crucial for the enhanced selectivity of this catalyst, in the liquid-phase Beckmann rearrangement.

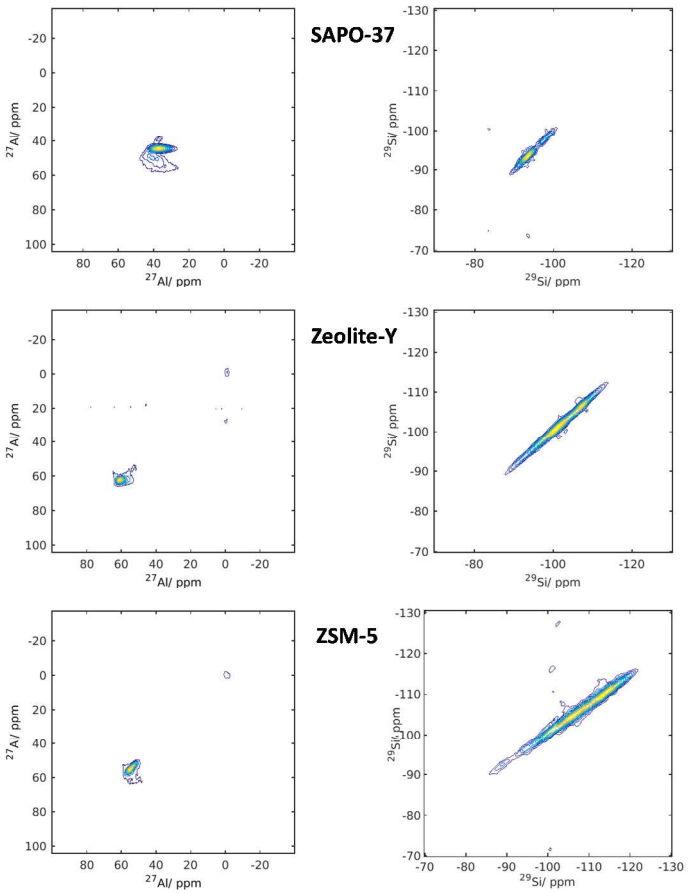

Figure 4 2D MAS ^{27}Al and ^{29}Si NMR spectra for the zeotypes.

Solid-state MAS NMR spectroscopy probes the local structural environment of framework atoms. The bulk AlPO matrix of SAPO-37 was affirmed through ^{31}P (Figure S5) and ^{27}Al MAS NMR (Figures 4 and S6, Table S2). ^{31}P MAS NMR showed one well resolved peak at -27 ppm, attributed to P(OAl)$_4$. The 1D ^{27}Al MAS NMR of SAPO-37 shows a broad peak at 33 ppm, with limited evidence of octahedral aluminium species at ~ 0 ppm. The ^{29}Si nuclei shows a broad signal, with an apex at -91 ppm (Figure S7), suggesting that the majority of silicon has formed Si(OAl)$_4$ species, confirming the incorporation of silicon into the material,[41] *via* type II substitution (Si replacing P).[7] 2D homonuclear MAS NMR (Figure 4) provides further resolution on the ^{27}Al and ^{29}Si NMR spectra.[42] The broad 1D ^{27}Al peak is a combination of two signals,

attributed to $Al(OP)_4$ and $Al(OP)_3(OSi)$, which arises from the isomorphous substitution of silicon into the framework.[43] The additional sharp peak in the 3QMAS spectrum is small and is compatible with a tetrahedrally-coordinated Al, possibly a surface defect site, such as $Al(OP)_3(OH)$ (Figure 4 and Table S2). Similarly the ^{29}Si spectra were deconvoluted into two peaks at -91 and -98 ppm, attributable to $Si(OAl)_4$ and $Si(OAl)_3(OSi)$, respectively, providing evidence for the formation of small silicon islands (Table S2). The ^{29}Si spectra of Zeolite-Y and ZSM-5 show two different environments, confirmed by 2D MAS NMR (Figure 4). The lower signal (-111 ppm in ZSM-5 and -106 ppm in Zeolite-Y) can be attributed to bulk $Si(OSi)_4$ different framework topologies.[44,45] The second signal (-105 ppm in ZSM-5 and -101 ppm in Zeolite-Y) is due to the presence of $Si(OSi)_3(OH)$ and $Si(OAl)(OSi)_3$ species. The latter confirms that aluminium has undergone isomorphous substitution and resides within the framework.[44] Al incorporation is further demonstrated through ^{27}Al NMR spectra for ZSM-5 and Zeolite-Y. Both species show a large fraction of framework-incorporated Al atoms, as evidenced by signals in the region of 54 - 62 ppm, which are attributed to $Al(OSi)_4$ species, with a further signal at 0 ppm, attributed to extra-framework octahedral Al sites (Figure 4), both in good agreement with published literature.[46,47] The acid sites were investigated using NH_3-TPD (Figure S8 and Table S3) and low-temperature, CO probe FT-IR (Figures 5 and Figures S9-S13 and Table S4). Both zeolites show significant quantities of defect silanol species (3750 cm^{-1}, Figure S9), which induce weak acidity,[48,49] as confirmed from the NH_3-TPD spectra of Zeolite-Y and ZSM-5 (silanol signal at 270 ^oC Figure S8). SAPO-37 does not have a Si-OH feature, though minor amounts of Al-OH/P-OH defect species are present (Figure S9).[50] In agreement with the NMR, Al-OH species are present to a small extent in Zeolite-Y and ZSM-5, though are unlikely to influence the reactivity of the catalysts. FT-IR further confirms the presence of Si-OH-Al

Brønsted acid species, from incorporation of the dopant atoms into the framework. The signal from Zeolite-Y and SAPO-37 is split into two characteristic bands, assigned to protons residing in supercages and sodalite cages of the faujasite system. Protons in ZSM-5 only occupy the 1-dimensional channel, thus a single Si-OH-Al band is observed. These findings indicate that the SAPO-37 catalyst is distinct from its zeolitic counterparts, in possessing a higher fraction of isolated Brønsted acid sites, owing to the lack of silicon island formation, and is conspicuous for its lack of defect silanols, resulting in uniform acidity.

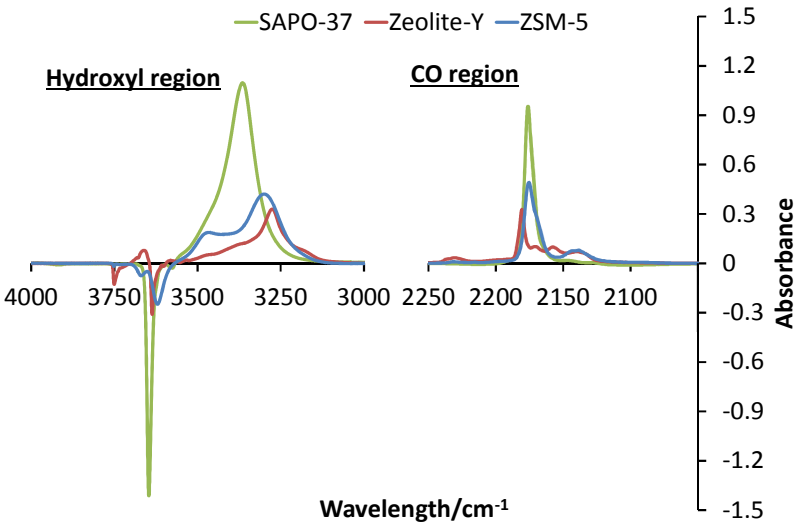

Figure 5 FT-IR difference spectra for low-temperature CO adsorbed on: SAPO-37 (green), Zeolite-Y (red) and ZSM-5 (blue), showing the decline of hydroxyl groups, and a shift to lower wavenumbers in the hydroxyl region, with an increase in the CO stretching region showing the binding to the Brønsted acid species.

The proton band (hydroxyls) shifted on adsorption of CO (Figures S10 and S11), where the magnitude of the shift correlates with acid site strength. Both zeolites possess stronger acid sites than SAPO-37, which was independently verified with NH_3-TPD (Figure S8).[51] The CO stretching region (2250-2100 cm^{-1}, Figure 5, S12 and S13) reveals that the zeolites possess some

moderate and strong Lewis acidity (2200 cm^{-1} and 2230 cm^{-1}, respectively).[51,52] These sites have been shown to induce cyclohexanone formation in the Beckmann rearrangement.[53] Quantifying the values from the CO stretching peaks (Table S4) and from the area values in the NH_3-TPD (Table S3), show that the total quantity of acid sites follows the trend: SAPO-37 > ZSM-5 > Zeolite-Y, despite similar dopant levels.

Table 1 Integrated peak areas and calculated acidity for the collidine-probed FT-IR.

	Integrated peak areas/(au/mg)				Total acidity/(mmol/g)			
System	**Weak**	**Medium**	**Strong**	**Total**	**Weak**	**Medium**	**Strong**	**Total**
SAPO-37	0.913	2.845	1.609	5.367	0.070	0.219	0.124	0.413
Zeolite-Y	0.625	0.806	1.259	2.690	0.048	0.062	0.097	0.207
ZSM-5	0.100	0.083	0.039	0.222	0.008	0.006	0.003	0.017

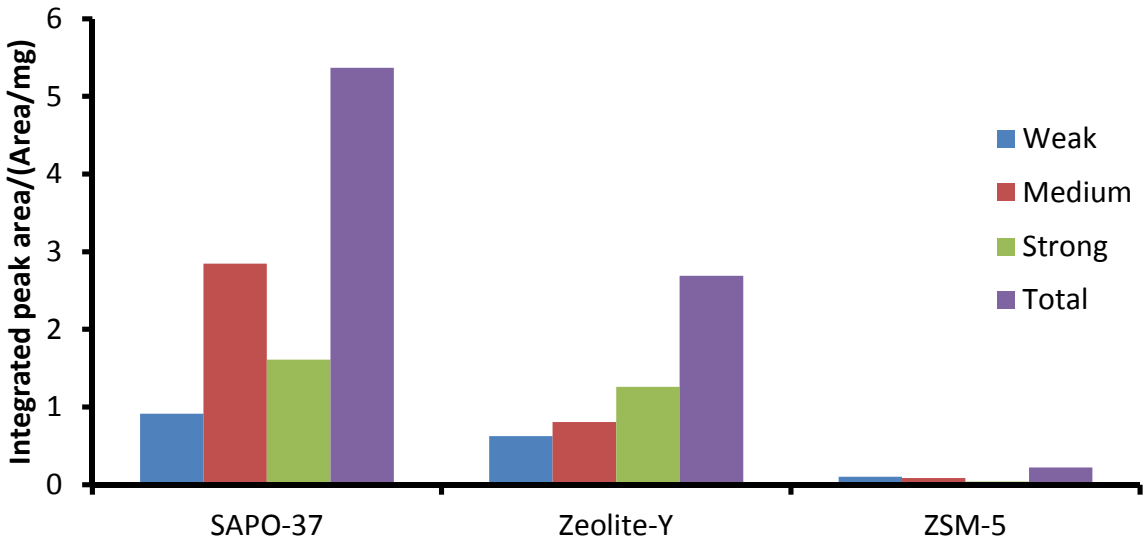

Figure 6 Summary of collidine FT-IR data for zeotype materials, highlighting the accessibility of the faujasite frameworks, with SAPO-37 possessing a high fraction of medium strength acid sites, whereas Zeolite-Y has a greater proportion of strong acid sites. The collidine probe is unable to access the ZSM-5 micropores leading to significantly fewer acid sites.

The QENS study has already shown that cyclohexanone oxime is able to access the internal sites of SAPO-37 and Zeolite-Y, but not ZSM-5. Although CO-probed FT-IR is able to probe the total acidity, a bulkier probe such as collidine was subsequently employed to identify selectively the acid sites that are accessible to the oxime. The latter should correspond to the vast majority of acid sites in the SAPO-37 and Zeolite-Y catalysts, but interaction can also be envisaged with acid sites located at the pore-mouth and extremities of ZSM-5 (Figures S14-S19). Both hydroxyl peaks in SAPO-37 and Zeolite-Y decrease on collidine adsorption, confirming that both supercage and sodalite cage protons are accessible: proton migration occurs at elevated temperatures (Figures S14, S16 and S18), or as collidine interacts with protons in the windows of the sodalite cages (most likely a through-space interaction since collidine is too large to occupy these cages). Integrating the area of the collidine doublet at 1637 and 1652 cm^{-1} quantifies the number of *accessible* sites (Figures S15, S17 and S19 and Table 1).[52] Despite ZSM-5 possessing a higher quantity of acid sites than Zeolite-Y (TPD and FTIR), the framework topology impedes access of the collidine probe and consequently, only surface silanol species and those in the vicinity of the pore-mouths are available for catalysis in ZSM-5 (Figure S15, S17 and S19). SAPO-37 and Zeolite-Y possess more accessible sites and it was observed that, although SAPO-37 has a greater overall acidity (Table 1 and Figure 6), Zeolite-Y has distinctly stronger acid sites, in agreement with NH_3-TPD and low-temperature, CO probed FT-IR findings.[15] The collidine results were in relatively good agreement with those obtained by NH_3-TPD and those

expected from the dopant loading (Table S5). The total acidity from collidine FTIR were generally lower than those found experimentally through NH_3-TPD, however this is likely due to the difference in size between the probes, with the bulkier collidine probe blocking neighbouring acid sites from other collidine molecules.[5,7,8] The NH_3-TPD for SAPO-37 is in excellent agreement with that predicted from the Si dopant loading (Table S5).[5,7,8] The ZSM-5 and Zeolite-Y NH_3-TPD values are significantly lower than those predicted from Al dopant loading. This is likely due to aluminium islanding and the formation of non-isolated sites.

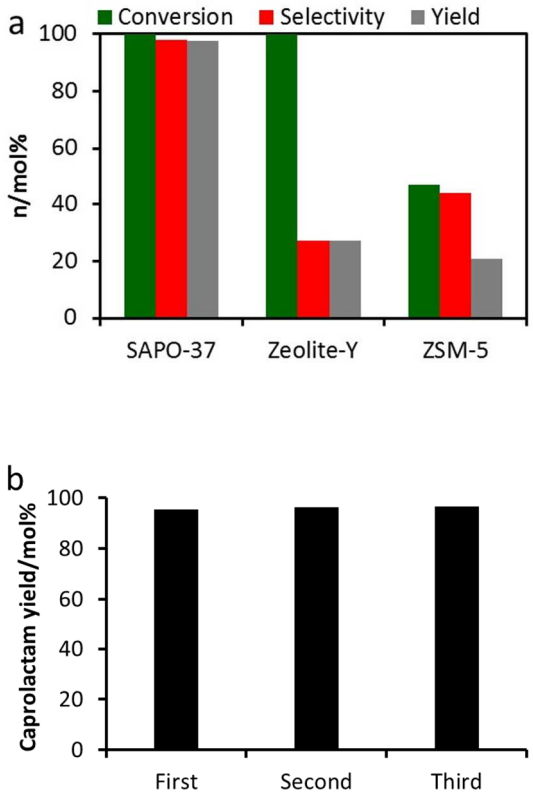

Figure 7 Liquid-phase Beckmann rearrangement data of cyclohexanone oxime. a) Highlighting the interplay between framework topology, active-site engineering and molecular diffusion. b) Showing consistent caprolactam yields from SAPO-37 on multiple regenerations, vindicating the reusability of the catalyst. See supporting information for experimental details.

The spectroscopic data reinforces the importance of combining the desired active site with the appropriate framework topology, which is further exemplified in the observed catalytic trends for the liquid-phase Beckmann rearrangement. The catalytic data (Figures 7a and 7b) shows notable trends that reflect the importance of the framework topology and acid-site strength, notwithstanding the critical role of diffusion and interaction of the substrate with the desired active-site. The faujasitic frameworks (SAPO-37 and Zeolite-Y) show equivalent levels of conversion, which vastly exceed that of ZSM-5 (47 mol%, Figure 7a). This trend is not commensurate with the total (measured) acidity (Figure S8 and Table S3), and therefore other factors are responsible for this remarkable finding.

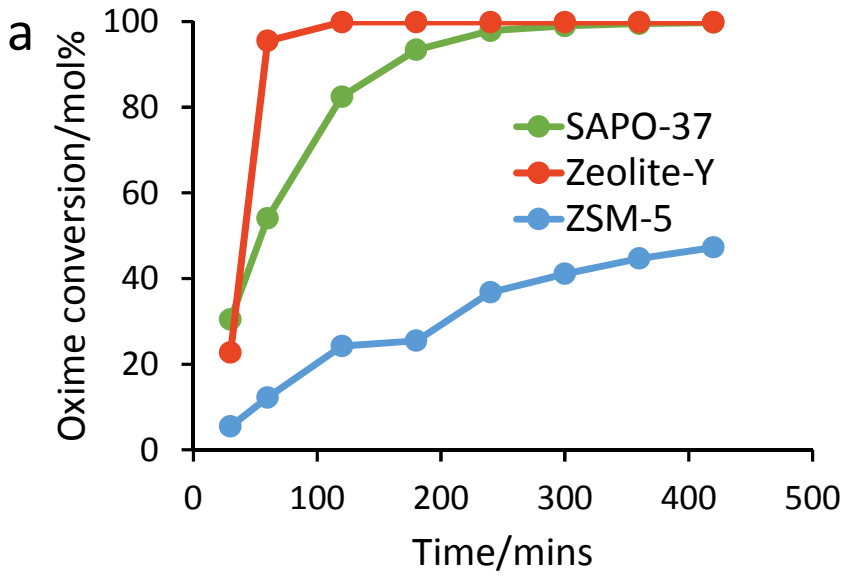

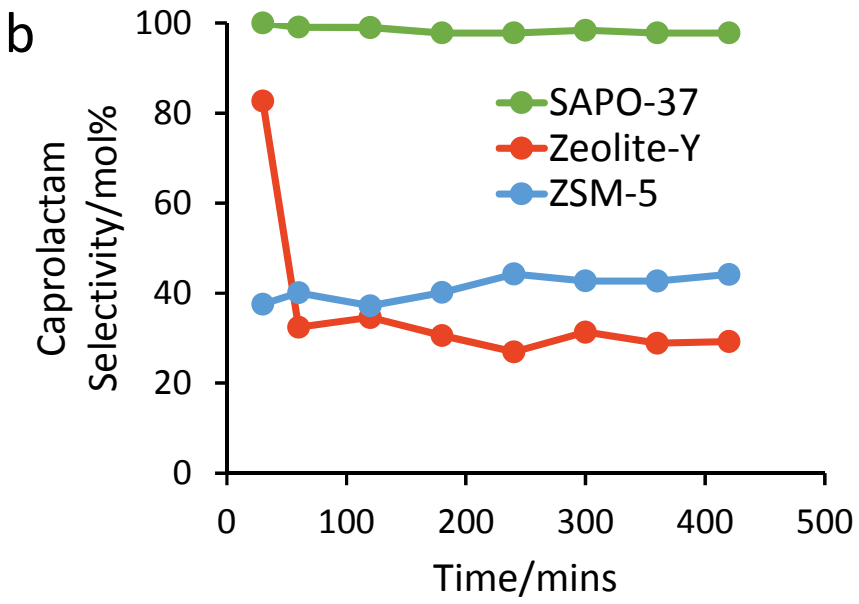

Figure 8 Liquid-phase Beckmann rearrangement data of cyclohexanone oxime showing the kinetic behaviour of a) conversion, and b) selectivity. See supporting information for experimental details.

Despite having fewer acid sites than both ZSM-5 and SAPO-37, kinetic studies have shown that Zeolite-Y displays a superior rate of conversion of the cyclohexanone oxime substrate (Figures 8a and 8b), although selectivity for caprolactam is low (Figure 8b). These findings are noteworthy and justify our hypothesis that the 'jump diffusion' observed in SAPO-37 originates from favourable catalyst-substrate interactions that are intrinsic to a specific acid site and independent of total acidity. The minimal Lewis acidity in the SAPO-37 species may also be a contributing factor, however, this does not contradict the QENS observations.[51,52] The QENS results (Figures 2 and S3) unequivocally reveal that, unlike the faujasitic systems, cyclohexanone oxime cannot permeate into the micropores of ZSM-5 over the timescales investigated, further substantiating that catalytic selectivity to the desired product, caprolactam, relies primarily on accessible internal acid sites. ZSM-5 has accessible acid sites only on the surface and at the pore

mouths, which impede both reactivity (because of hindered diffusion) and selectivity for ε-caprolactam (Scheme 1). As Zeolite-Y possesses a greater proportion of 'stronger' acid sites (Table 1 and Figure 6) than SAPO-37, the formation of undesired side-products is favoured,[53] in stark contrast to the (desired) weaker sites in SAPO-37. It is therefore remarkable that, while both Zeolite-Y and SAPO-37 display high conversions in the liquid-phase process (Figure 7a and 8a), we did not observe any notable interactions with the oxime molecule in the QENS experiments for Zeolite-Y (Figure 2a and Figure S4). These combined findings are therefore crucial in highlighting the importance of the favourable interactions of the internal acid sites in the SAPO-37 catalyst with the cyclohexanone oxime substrate, which lead to the highly selective formation of caprolactam in the liquid-phase at low temperatures (Figures 7a and 8b). These internal acid sites are very stable and can be regenerated to deliver consistent caprolactam yields over several cycles, thereby confirming the recyclability and heterogeneity of the SAPO-37 catalyst (Figure 7b). The stability of the SAPO-37 catalyst was also evaluated post-catalysis. Powder XRD showed the faujasitic crystalline structure was retained post-catalysis and on reactivation (Figure S20). Similarly N_2 physisorption confirmed that the total pore volume of the material could be recovered on reactivation, with the micropore volume being completely retained (Table S6). Finally 1D ^{27}Al MAS NMR spectra (Figure S21) showed no variation between fresh, post-catalysis and reactivated SAPO-37 catalysts, either under nitrogen or on exposure to air for 12 hours. These findings, coupled with the catalytic data (multiple recycle tests, Figure 7b) demonstrate the stability of the SAPO-37 catalyst for this reaction.

These fundamental studies are of paramount importance in understanding the complex nature of the interplay between active-site, framework topology, and reaction pathways. Understanding these subtle structure-activity relationships and associated diffusion pathways will pave the way

for the industrial exploitation of the liquid-phase Beckmann rearrangement process, using heterogeneous solids.[15]

CONCLUSIONS

The ability to control precisely the nature and strength of solid-acid sites, combined with significant insights into molecular diffusion behaviour within nanoporous architectures, has led to important new insights into a novel catalytic system for the low-temperature, liquid-phase production of ε-caprolactam (precursor to Nylon-6). Neutron scattering (QENS and INS), in combination with aligned spectroscopic techniques, offers unique insights into the distinct role of surface and internal acid sites and their mechanistic influence in the liquid-phase Beckmann rearrangement of cyclohexanone oxime with FAU and MFI catalysts. This study further elucidates the contrasting diffusion and catalytic pathways that are prevalent within these heterogeneous solids, and highlights the interplay of framework topology and active site design in sustainable catalysis.

ASSOCIATED CONTENT

Supporting Information. Full synthesis, characterization and catalytic methodologies available. Also basic QENS background theory and further textural, neutron scattering, NMR, TPD and FT-IR data available are available in the supporting information. This material is available free of charge via the Internet at http://pubs.acs.org.

AUTHOR INFORMATION

Corresponding Author: Robert Raja: R.Raja@soton.ac.uk

Author Contributions: The manuscript was written through contributions of all authors.

Funding Sources

The UK Catalysis Hub is funded by EPSRC (Engineering and Physical Sciences Research Council) *via* grants EP/K014706/1, EP/K014668/1, EP/K014854/1, EP/K014714/1 and EP/M013219/1. The EPSRC also funded the Centre for Doctoral Training scheme with grant no. EP/G036675/1. The project was also funded by the Science and Technologies Facilities Council and ISIS Pulsed Neutron Muon Source. MEP, SHN and SC also acknowledge Honeywell LLC for studentship.

ACKNOWLEDGMENT

The UK Catalysis Hub is kindly thanked for resources and support provided *via* our membership of the UK Catalysis Hub Consortium. We thank the STFC Rutherford Appleton Laboratory and ISIS Pulsed Neutron and Muon Source for access to neutron beam facilities.

REFERENCES

1. Liebgott, P. P.; Leroux, F.; Burlat, B.; Dementin, S.; Baffert, C.; Lautier, T.; Fourmond, V.; Ceccaldi, P.; Cavazza, C.; Meynial-Salles, I.; Soucaille, P.; Fontecilla-Camps, J. C.; Guigliarelli, B.; Bertrand, P.; Rousset M.; Léger, C. *Nat. Chem. Bio.* **2010**, *6*, 63-70.

2. Forneris, F.; Mattevi, A. *Science* **2008**, *321*, 213-216.

3. Jiang, J.; Jorda, J. L.; Yu, J.; Baumes, L. A.; Mugnaioli, E.; Diaz-Cabanas, M. J.; Kolb U.; Corma, A. *Science* **2011**, *333*, 1131-1134.

4. Choi, M.; Na, K.; Kim, J.; Sakamoto, Y.; Terasaki, O.; Ryoo, R. *Nature* **2009**, *461*, 246-249.

5. Raja, R.; Potter, M. E.; Newland, S. H. *Chem. Commun.* **2014**, *50*, 5940-5957.

6. Choi, M.; Cho, H. S.; Srivastava, R.; Venkatesan, C.; Choi, D. H.; Ryoo, R. *Nat. Mater.* **2006**, *5*, 718-723.

7. Potter, M. E; Cholerton, M. E.; Kezina, J.; Bounds, R.; Carravetta, M.; Manzoli, M.; Gianotti, E.; Lefenfeld, M.; Raja, R. *ACS Catal.* **2014**, *4*, 4161-4169.

8. Gianotti, E.; Manzoli, M.; Potter, M. E.; Shetti, V. N.; Sun, D.; Paterson, J.; Mezza, T. M.; Levy A.; Raja R. *Chem. Sci.* **2014**, *5*, 1810-1819.

9. Dusselier, M.; Van Wouwe, P.; Dewaela, A.; Jacobs, P. A.; Sels, B. F. *Science* **2015**, *349*, 78-80.

10. Spangsberg Holm, M.; Saravanamurugan, S.; Taarning, E. *Science* **2010**, *328*, 602-605.

11. Leithall, R. M.; Shetti, V. N.; Maurelli, S.; Chiesa, M.; Gianotti, E.; Raja, R. *J. Am. Chem. Soc.* **2013**, *135*, 2915-2918.

12. Paterson, J.; Potter, M. E.; Gianotti, E.; Raja, R. *Chem. Commun.* **2011**, *47*, 517-519.

13. Buurmans, I. L. C.; Ruiz-Martínez, J.; Knowles, W. V.; van der Beek, D.; Bergwerff, J. A.; Vogt, E .T. C.; Weckhuysen, B. M. *Nat. Chem.* **2011**, *3*, 862-867.

14. Lefenfeld, M.; Raja, R.; Paterson, A. J.; Potter, M. E. *US Patent* US 9,012,709*,* **2015**.

15. Levy, A. B.; Raja, R.; Potter, M. E. *US Patent* US 9,221,762, **2015**.

16. Maurelli, S.; Vishnuvarthan, M.; Chiesa, M.; Berlier, G.; Van Doorslaer, S. *J. Am. Chem. Soc.* **2011**, *133*, 7340-7343.

17. Han, O. H.; Kim, C. S.; Hong, S. B. *Angew. Chem. Int. Ed.* **2002**, *41*, 469-472.

18. "Nylon – A global strategic business report" *Global industry analysts inc.,* **2010**.

19. Chmelik, C.; Karger, J. *Chem. Soc. Rev.* **2010**, *39*, 4864-4884.

20. Forni, L.; Fornasari, G.; Giordano, G.; Lucarelli, C.; Katovic, A.; Trifiro, F.; Perri, C.; Nagy, J. B. *Phys. Chem. Chem. Phys.* **2004**, *6*, 1842-1847.

21. Flego, C.; Dalloro, L. *Micropor. Mesopor. Mater.* **2003**, *60*, 263-271.

22. Izumi, Y.; Ichihashi, H.; Shimazu, Y.; Kitamura, M.; Sato, H. *Bull. Chem. Soc. Jpn.* **2007**, *80*, 1280-1287.

23. Marie, O.; Thibault-Starzyk, F.; Massiani, P. *J. Catal.* **2005**, *230*, 28-37.

24. Camblor, M. A.; Corma, A.; Garcia, H.; Semmer-Herldedan, V.; Valencia, S. *J. Catal.* **1998**, *177*, 267-272.

25. Fernandez, A. B.; Lezcano-Gonzalez, I.; Boronat, M.; Blasco, T.; Corma A. *J. Catal.* **2007**, *249,* 116-119.

26. Heitmann, G. P.; Dahlhoff, G.; Hoelderich, W. F. *J. Catal.* **1999**, *186*, 12-19.

27. Jobic, H.; Theodorou, D. N. *Micropor. Mesopor. Mater.* **2007**, *102*, 21-50.

28. O'Malley, A. J.; Parker, S. F.; Chutia, A.; Farrow, M. R.; Silverwood, I. P.; Garcia-Sakai V.; Catlow, C. R. A. *Chem. Commun.* **2016**, *52*, 2897-2900.

29. Schuster C.; Hoelderich, W. F. *Catal. Today* **2000**, *60*, 193-207.

30. Treacey, M. M. J.; Higgins, J. B. Collection of simulated XRD powder patterns for Zeolites, Elsevier Science and Technology, 5th edn. **2007**.

31. Fick, A. Ueber Diffusion. *Ann. Phys. Chem.* **1855**, *94*, 59-86.

32. van Hove, L. *Phys. Rev.*, **1954**, *95*, 249-262.

33. Jobic, H.; Fitch, A. N.; Combet, J. *J. Phys. Chem. B* **2000**, *104*, 8491-8497.

34. Sahasrabudhe, A.; Mitra, S.; Tripathi, A. K.; Mukhopadhay, R.; Gupta, N. M. *Phys. Chem. Chem. Phys.* **2003**, *5*, 3066-3075.

35. http://dx.doi.org/10.5286/SOFTWARE/MANTID

36. Mukhopadhyay, S.; *RAL Technical Report*, RAL-TR-2014-005, **2014**.

37. Jobic, H.; Bee, M.; Pouget, S. *J. Phys. Chem. B* **2000**, *104*, 7130-7133.

38. Auerbach, S. M.; Henson, N. J.; Cheetham, A. K.; Metiu, H. I. *J. Phys. Chem.* **1995**, *99*, 10600-10608.

39. Segall, M. D.; Lindan, P. J. D.; Probert, M. J.; Pickard, C. J.; Hasnip, P. J.; Clark, S. J.; Payne, M. C. *J. Phys. Condens. Mater.* **2002**, *14*, 2717-2744.

40. Clark, S. J.; Segall, M. D.; Pickard, C. J.; Hasnip, P. J.; Probert, M. J.; Refson, K.; Payne, M. C. *Z. Krist.* **2005**, *220*, 567-570.

41. Sastre, G.; Lewis, D. W.; Catlow, C. R. A. *J. Phys. Chem. B* **1997**, *101*, 5249-5262.

42. Kobera, L.; Brus, J.; Klein, P.; Dedecek, J.; Urbanova, M. *Solid State Nucl. Magn. Reson.* **2014**, *57-58*, 29-38.

43. Chen, T. H.; Wouters, B. H.; Grobet, P. J. *J. Phys. Chem. B* **1999**, *103*, 6179—6184.

44. Fyfe, C. A.; Feng, Y.; Grondey, H.; Kokotailo, G. T.; Gies, H. *Chem. Rev.* **1991**, *91*, 1525-1543.

45. Zhang, W.; Bao, X.; Guo, X.; Wang, X. *Catal. Lett.* **1999**, *60*, 89-94.

46. Jiao, J.; Kanellopoulos, J.; Wang, W.; Ray, S. S.; Foerster, H.; Freude, D.; Hunger, M. *Phys. Chem. Chem. Phys.* **2005**, *7*, 3221-3226.

47. Rocha, J.; Carr, S. W.; Klinowski, J. *Chem. Phys. Lett.* **1991**, *187*, 401-408.

48. Gianotti, E.; Bisio, C.; Marchese, L.; Guidotti, M.; Ravasio, N.; Psaro, P.; Coluccia, S. *J. Phys. Chem. C* **2007**, *111*, 5083-5089.

49. Markova, M. A.; Ojo, A. F.; Karim, K.; Hunger, M.; Dwyer, J. *J. Phys. Chem.* **1994**, *98*, 3619-3623.

50. Bordiga, S.; Lamberti, C.; Geobaldo, F.; Zecchina, A.; Turnes Palomino, G; Otero Arean, C. *Langmuir* **1995**, *11*, 527-533.

51. Chakarova K.; Hadjiivanov, K. *J. Phys. Chem. C* **2011**, *115*, 4806-4817.

52. Spangsberg Holm, M.; Svelle, S.; Joensen, F.; Beato, P.; Christensen, C. H.; Bordiga S.; Bjorgen, M. *Appl. Catal. A: Gen.* **2009**, *356*, 23-30.

53. Ngamcharussrivichai, C.; Wu, P.; Tatsumi, T. *J. Catal.* **2005**, *235*, 139-149.

Insert Table of Contents Graphic and Synopsis Here